J Bionic Eng 15 (2018) 471–480
DOI: https://doi.org/10.1007/s42235-018-0038-4

Journal of Bionic Engineering
http://www.springer.com/journal/42235

Operculum of a Water Snail is a Hydrodynamic Lubrication Sheet

Xiaoyan Xu[1], Jianing Wu[2,3], Yunqiang Yang[1*], Rengao Zhu[1], Shaoze Yan[2,3*]

1. *School of Engineering and Technology*, *China University of Geosciences* (*Beijing*), *Beijing* 100083, *China*
2. *Division of Intelligent and Biomechanical Systems*, *State Key Laboratory of Tribology*, *Tsinghua University*, *Beijing* 100084, *China*
3. *Department of Mechanical Engineering*, *Tsinghua University*, *Beijing* 100084, *China*

Abstract

Water snails developed a distinct appendage, the operculum, to better protect the body against predators. When the animal is active and crawling, part of the underside of the shell rests on the outer surface of the operculum. We observed the water snails (*Pomacea canaliculata*) spend ~3 hours per day foraging, and the relative angular velocity between the shell and operculum can reach up to 10 $^{\circ}\cdot s^{-1}$, which might inevitably lead to abrasion on the shell and operculum interface. However, by electron microscopy images, we found that the underside of the shell and outer surface of the operculum is not severely worn, which indicates that this animal might have a strategy to reduce wear. We discovered the superimposed rings distributed concentrically on the surface, which can generate micro-grooves for a hydrodynamic lubrication. We theoretically and experimentally revealed the mechanism of drag reduction combing the groove geometry and hydrodynamics. This textured operculum surface might provide a friction coefficient up to 0.012 as a stability-resilience, which protects the structure of the snail's shell and operculum. This mechanism might open up new paths for studies of micro-anti-wear structures used in liquid media.

Keywords: water snails, operculum, micro-grooves, friction reduction, biomaterial

1 Introduction

Water snails are omnivorous, feeding on periphyton, macrophytes, detritus and animal matter[1]. Seuffert *et al*. showed that *P*. *canaliculata* spends 60.7% of the time on feeding at 25 ˚C, and the percentage of time spending on crawling (averaging 20.2%) is not affected by temperature[2]. The long periods of time spent moving might cause wear in animal appendages or even severely lead to death. The operculum of a water snail is the appendage that attached to the upper surface of the foot and secreted by specific gland cells[3]. When a water snail moves and crawls, it put their shell on the outer surface of the operculum. But when the snail is threatened (*e*.*g*., a predator is encountered or drought)[4,5], it folds foot and retracts the soft body to shell by muscle contractions. However, there are no obvious wear scars in the contact area of the shell and operculum. The microstructure of animals exhibit excellent biomechanical properties[6–9]. Investigations revealed that a large number of insects, land and aquatic animals and seashells have evolved non-smooth surfaces exhibiting adaptive properties of drag reduction and anti-wear[10]. For instance, miniature ridges on honeybee's galeae can significantly reduce drag during nectar-dipping[11]. The glossa of the honeybee erect hairs in a specific pattern can reduce the resistance in nectar feeding[12,13]. Earthworms can reduce adhesion between the body surface and the surrounding soil by annular somite[14]. Shark skin is covered by individual tooth-like scales which contribute to a low drag coefficient while swimming[15]. In recent years, techniques of reducing friction inspired by functional appendages of animals made a variety of progresses[16–20]. However, there are no studies that have revealed the effect of microstructure on the friction reduction of the water snail's operculum.

This paper focuses on the contradictive conditions between long-term rotation in operculum's and none wear between interfaces. We investigated three species of water snails. According to the micro-grooves structure of the operculum, we establish a theoretical model for hydrodynamic lubrication to elucidate the friction reduction mechanism in the operculum. The model might provide methodologies for engineering applications on designing and fabricating micro-anti-wear structure.

***Corresponding author:** Yunqiang Yang; Shaoze Yan
E-mail: cugbyyq@163.com; yansz@mail.tsinghua.edu.cn

2 Materials and methods

2.1 Water snail husbandry

P. canaliculata were collected in Guilin, Guangxi province, China (25.29 ˚N, 110.28 ˚E). *Pomacea bridgesii* were collected in Dalian, Liaoning province, China (38.92 ˚N, 121.62 ˚E). *Bellamya chinensis* were collected from Dongting Lake, Hunan province, China (29.37 ˚N, 113.09 ˚E). Then they were transported to China University of Geosciences (Beijing) and fed in the laboratory (Figs. 1a and 1b). Three species of water snails were placed in a glass tank (200 mm × 140 mm × 170 mm) with freshwater respectively (n = 20 snails, each species), and the water was changed per three days. The glass tank was equipped with an artificial heater to maintain the water temperature at 26 ˚C. Water snails were fed with green vegetables, and they could move freely within the tank (Fig. 1c).

2.2 Movement observation

To obtain the experimental data referring to the angular displacement between the operculum and the shell, three species of water snails with different sizes were selected, and their movements were filmed using video camera (EOS 5D Mark II, Canon, Japan) with 1080 pixels progressive scanning. As shown in Fig. 1d, the video camera was put on a height positioner and the water snail was placed in a glass tank with freshwater. An illuminator was used to adjust the brightness, and the crawling process was recorded at a frame rate of 30 fps. Furthermore, in another experiment, we applied a microscope (CX 31, Olympus, Japan) equipped with a high-speed camera (Phantom M110, USA) to observe the contact state between the operculum and the shell. To ensure the water snails remained natural state, the water snails were placed in a plastic dish with water. While the water snails crawled up the vertical wall, the contact state between the operculum and the shell was captured by the high-speed camera at a frame rate of 30 fps.

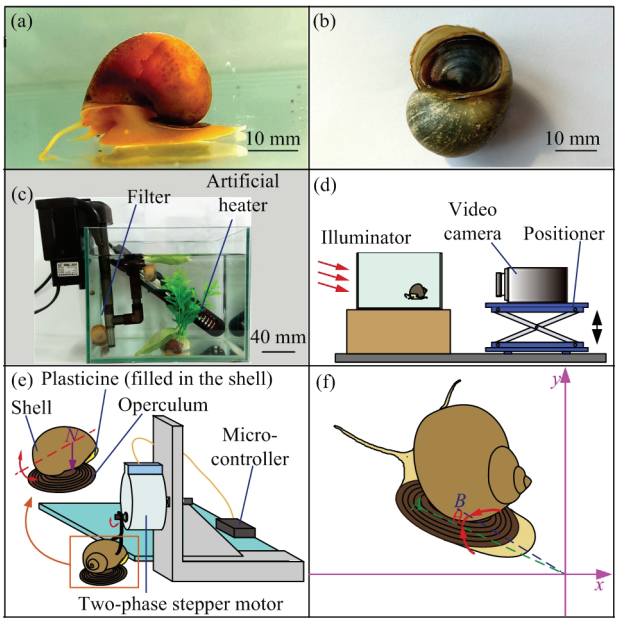

Fig. 1 Water snail, tank for observation, experimental setups and kinematic measurement. (a) A water snail crawling in a lateral view (*P. canaliculata*); (b) the state of a snail which retracts its soft body into the shell (*P. canaliculata*); (c) photograph of observation tank; (d) experimental setup for crawling recordings; (e) the setup for dry friction experiment; (f) schematic illustration of the definition of parameter θ.

2.3 Postmortem examination of operculum and underside shell

To examine the surface morphology of the water snail's operculum, five opercula of each species were observed under an optical microscope (Eclipse 90i, Nikon, Japan) at a resolution of 0.05 μm. Then eight opercula and three underside shells (*P. canaliculata*) were prepared for Scanning Electron Microscope (SEM). They were first washed by 100% acetone then dehydrated by pure ethanol for three times and 8 minutes each time. Next, five opercula were cut through the middle in order to observe the morphology of the operculum's cross-section. Then the samples were natural air-dried, followed by oven drying at 60 ˚C for 48 hours. These samples were fixed on the SEM observation platform with graphite adhesive tapes. After the gold sputtering treatment (~10 nm), the samples were observed through SEM (FEI Quanta 200, Czech Republic). In addition, to obtain the three-dimensional morphology of the textured surface, total fifteen opercula (n = 5, each species) were observed by a three-dimensional white lighter interferometer (Nano Map-D, AEP Technology, USA) with a resolution of 0.01 nm.

2.4 Friction measurement

The dry friction experiments, including simulation of dry friction between the shell and operculum, observation of surface micro-morphology of wear scars, and measurement of the wear scars on the operculum were

conducted to simulate the condition of shell rotation on the operculum without water. This experiment only used *P. canaliculata*. The experimental setup for the dry friction experiment was comprised of a microcontroller, a two-phase stepper motor and a piece of wire (Fig. 1e). The operculum was fixed on the platform by using double-sided adhesive tape, and the shell was connected to the stepper motor shaft by a piece of wire which passes through the hole of the shell. The shell was adjusted to an appropriate height where the shell underside could contact with the operculum by adjusting the wire length. And 5 grams of plasticine was filled in the shell to increase the weight in order to accelerate wear. In addition, the speed and rotation degree of two-phase stepper motor was controlled by the microcontroller. The motor shaft rotated 30 degrees in clockwise direction then rotated in anticlockwise returning to the original place. This rotation was repeated constantly, and the rotation speed was 30 $^\circ \cdot s^{-1}$. We defined a single process as a friction cycle, which cycle took 2 sec. We used C to represent the number of friction cycles.

The dry friction experiment was carried out for 13 h ($C = 23400$) in the ambient air (26 ˚C ± 1 ˚C and 53 ± 2% RH, 1 atm). The wear traces of the operculum were observed by metallographic microscope (BX 51M, Olympus, Japan). In addition, the surface roughness was measured by three-dimensional white lighter interferometer (Nexview, zygo, USA) after 5 minutes of ethanol ultrasonic surface cleaning to remove the debris covered on the scars.

2.5 Kinematics

The videos captured from movement observation were analyzed frame by frame. For statistical analyses, two points were marked on the operculum and the shell, respectively. The coordinates of the marker points were obtained by the software Tracker (V4.91, Open Source Physics, USA). The relative angular velocity was identified by analyzing the coordinates of the marker points. In the coordinate system, the two marker points as A and B have coordinates $A(x_1,y_1)$, $B(x_2,y_2)$. The parameter θ is defined as the angle between the two marked points, as shown in Fig. 1f. Therefore, θ can be expressed by:

$$\theta = (\arctan\frac{y_1}{x_1} + 180) - (\arctan\frac{y_2}{x_2} + 180). \quad (1)$$

Then the angle difference between the continuously two frames is the angular displacement $\Delta\theta_i$, furthermore, the average relative angular velocity $\bar{\omega}$ can be calculated as:

$$\bar{\omega} = \frac{\sum \Delta\theta_i}{\sum t_i} \quad (i = 1,2,3\cdots), \quad (2)$$

where i is the number of frames and t_i is the time interval of the continuously two frames.

3 Results and discussion

3.1 Morphology of the operculum

We observed the outer surface and cross-section morphology of the operculum and underside shell of the three species of water snails by a microscope and SEM. An operculum is shaped as an elliptical sheet with an outer concave depression and superimposed rings distributed concentrically on the surface (Figs. 2a and 2b). As shown in Figs. 2c and 2d, the annular micro-grooves are circled at the outer surface of the operculum. Notably, the microstructure architecture of the operculum is symmetrical and not seriously worn. The underside of the shell which contact with the operculum is not drastically worn either (Fig. 2e). Fig. 2f shows the three-dimensional morphology of the textured surface, which was captured by a three-dimensional white lighter interferometer. This image offers a further indication of the ring-like micro-grooves structure of the operculum. Comparison among micro-grooves of three water snail species is shown in Figs. 2b, 2g and 2h. We measured dimensional parameters of the micro-grooves by the software Digimizer (MedCalc Software, Belgium). For *P. canaliculata*, *P. bridgesii* and *B. chinensis*, these ridges on the outer surface of operculum were distributed with a spacing of 145 μm ± 30 μm (mean ± s.d.), 82 μm ± 17 μm, 57 μm ± 18 μm and with width of 85 μm ± 25 μm (mean ± s.d.), 55 μm ± 15 μm, 66 μm ± 20 μm, respectively. In addition, the average depth of the groove were 15 μm ± 4 μm (mean ± s.d.), 11 μm ± 4 μm and 14 μm ± 4 μm (n = 5 opercula, each species).

3.2 Kinematics

We found that *P. canaliculata* and *P. bridgesii* spend ~3 hours per day on crawling around to forage, and the frequency of reciprocating rotation between

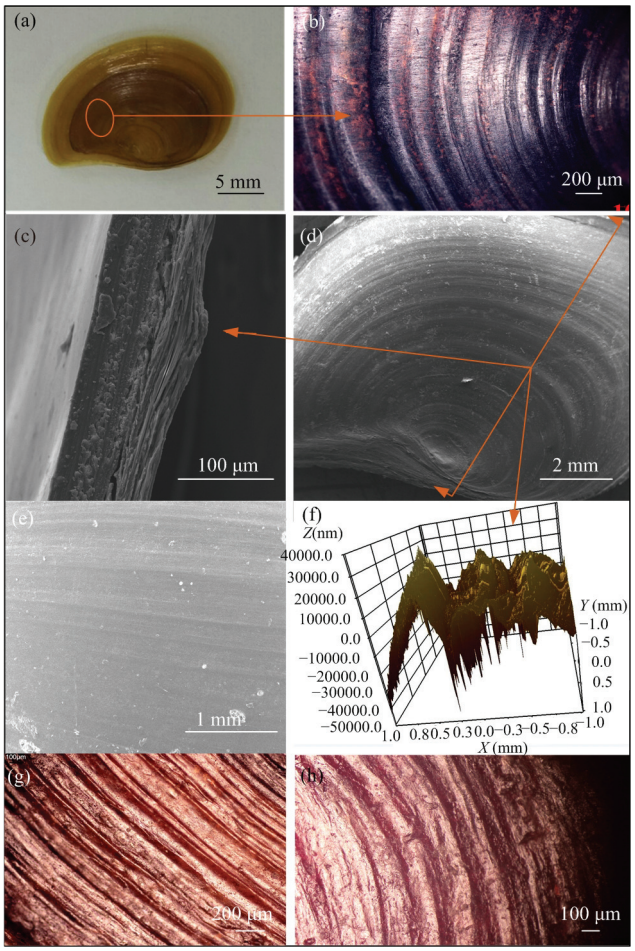

Fig. 2 Micro-morphology of the operculum and the shell. (a) Full view of the operculum of *P. canaliculata*; (b) zoomed-in view of the operculum's outer surface (*P. canaliculata*); (c) SEM image of the operculum's cross-section (*P. canaliculata*); (d) SEM image of the operculum's outer surface (*P. canaliculata*); (e) SEM image of the underside shell which contact the operculum (*P. canaliculata*); (f) the three-dimensional morphology image of the operculum (*P. canaliculata*); (g) optical microscope image of the operculum (*P. bridgesii*); (h) optical microscope image of the operculum (*B. chinensis*).

snail's shell and operculum was approximately 10 times per minute. Hence, the number of the relative rotation is close to a million times for a water snail with an average life expectancy of 1.5 years[21], which indicates that frequent friction might exist between the shell and operculum (see Supplementary Material movie S1). In addition, however, *B. chinensis* spend less time on crawling. Figs. 3a–3d show four typical events of a water snail's (*P. canaliculata*) crawling. These figures suggest that the angle variation between the operculum and the shell. We measured crawling distance s and angle θ with respect to time t by the software Tracker. Fig. 3e indicates an approximately linear mapping between s and t, so the crawling distance of a water snail increases continuously and smoothly with time goes. Moreover, the angle θ between the shell and operculum which further demonstrates the frequent angle variation of a water snail during crawling (Fig. 3e). The average relative angular velocity between the shell and operculum of *P. canaliculata*, *P. bridgesii* and *B. chinensis* are 2.52 $^{\circ}\cdot s^{-1}$, 1.67 $^{\circ}\cdot s^{-1}$ and 0.37 $^{\circ}\cdot s^{-1}$, respectively (n=3 snails, each species). For *P. canaliculata*, the maximum relative angular velocity can reach up to 10 $^{\circ}\cdot s^{-1}$. We observed a water film that separates the shell and operculum when the snail moves. We recorded that by a high-speed camera (see Supplementary Material movie S2).

3.3 Tribological properties

To illustrate the surface damage of the operculum induced by dry friction, we measured the surface

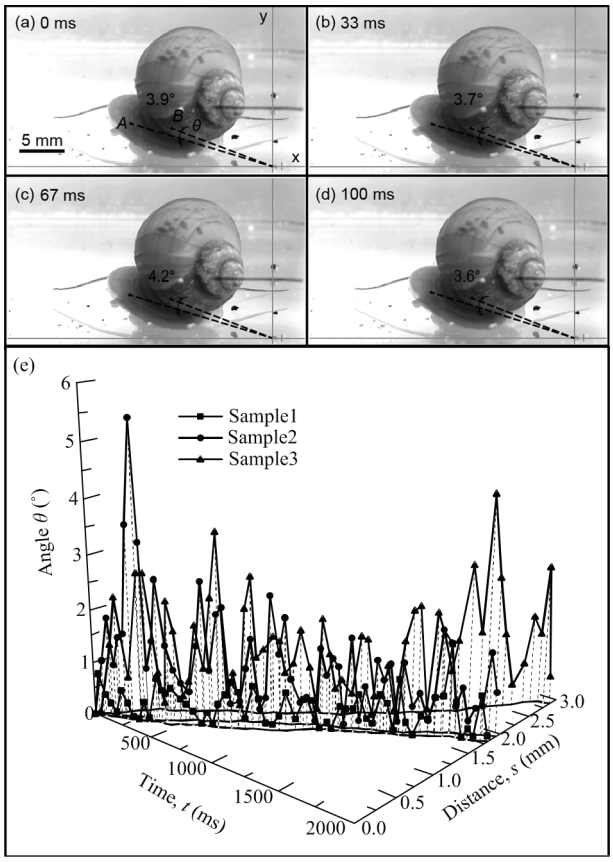

Fig. 3 The angle varies between the operculum and the shell (*P. canaliculata*). (a)–(d) The variations of angle θ of a water snail during crawling under water; (e) relationship between time t, crawling distance s and angle θ of 3 typical samples.

morphology and topography by a metallographic microscope and three-dimensional white lighter interferometer (Figs. 4a–4d). It can be found that the striated wear tracks were mainly concentrated on the middle area and the micro-ridges were nearly worn out (Figs. 4a and 4b). Moreover, Figs. 4c and 4d show the topography of operculum between before and after dry friction respectively. The surface becomes smoother after dry friction experiment as illustrated in Figs. 4a–4d. We extracted the red region (0 μm – 25 μm) and green region (−5 μm – −25 μm) respectively from Figs. 4c and 4d by tool box for image processing in Matlab (R2016a, MathWorks, USA) (Figs. 4e and 4f). In order to compare the change of areas of red and green after dry friction, the proportions of red and green areas were calculated, respectively. As shown in Fig. 4g, the proportion of red area decrease from 81.5% to 58.1% after dry friction, whereas the green area increase from 14.6% to 36.6%, which illustrate that the micro-ridges are nearly worn out and the sunken areas become gradually larger during the dry friction (Fig. 4h). During wearing, when the two surfaces contact each other, the asperities are slowly removed and the roughness value is reduced. By Chandrasekaran's theories[22], the transient wear rate depends on the surface roughness, and high initial surface roughness leads to a higher wear rate. We measured the arithmetic average of surface roughness (*Ra*) of operculum before and after dry friction respectively by using the white lighter interferometer, and found *Ra* decrease from 12.63 μm to 10.19 μm. The difference in surface roughness of the operculum is caused by dry friction which indicates that the snails might have a strategy to protect themselves from being worn between their shells and opercula.

3.4 Hydrodynamic model

According to observations, we speculate that the micro-grooves of the operculum might make the operculum and shell non-contact by a thin water film result from the hydrodynamic effect[23]. To validate that, one hydrodynamic model which considers the micro-grooves according to Reynolds equations[24] is established to reveal the friction reduction mechanism of the operculum. As shown in Fig. 5a, we simplify the underside shell as a curved surface and operculum as a sheet with micro-grooves. The micro-ridges on the operculum can be regarded as Rayleigh blocks[25]. The clearance between the shell and operculum is filled with water, which contributes to friction reduction, and the y direction flow is neglected during the calculation[10]. Moreover, the contact area between the underside shell and operculum is small, thus the curvature effects are negligible and movement between the shell and operculum can be equivalent to the linear motion in x direction (Fig. 5b). We define w_g as the width of the micro-groove, d_g as the depth of the micro-groove, w_r as the width of the micro-ridge and η as the viscosity of water at 26 ˚C. The thickness of water film, namely the distance between the shell and top of the micro-ridge, is h_b. We hypothesize that the shell is moved to right at a pace

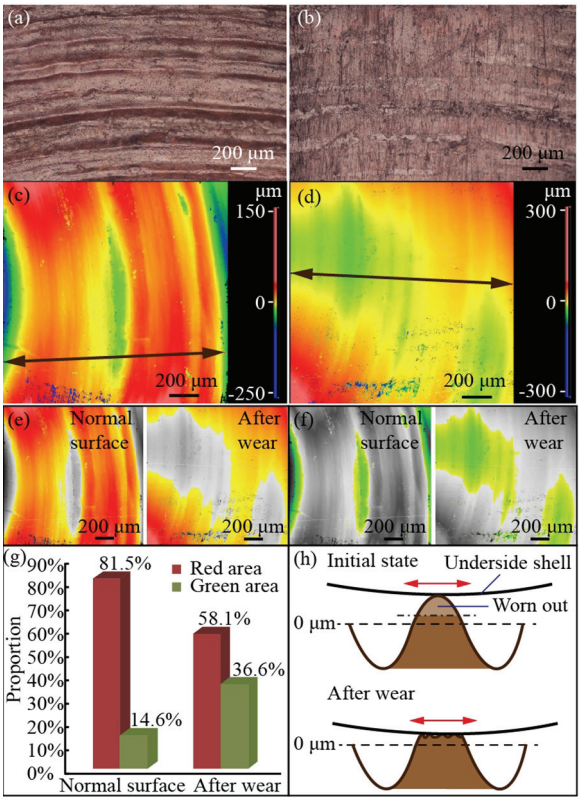

Fig. 4 Comparison of surface between fresh snail operculum samples and worn snail operculum samples. (a) Morphology of operculum of a fresh snail specimen; (b) the morphology of wear traces of operculum after dry friction experiment; (c, d) surficial topography of the operculum before (c) and after (d) dry friction experiment; (e) extraction of red area (0 μm – 25 μm) before and after dry friction experiment; (f) extraction of green area (−5 μm– −25 μm) before and after dry friction experiment; (g) bar graph of proportion of red and green area before and after dry friction; (h) schematic illustration of wear caused by dry friction for one micro-ridge.

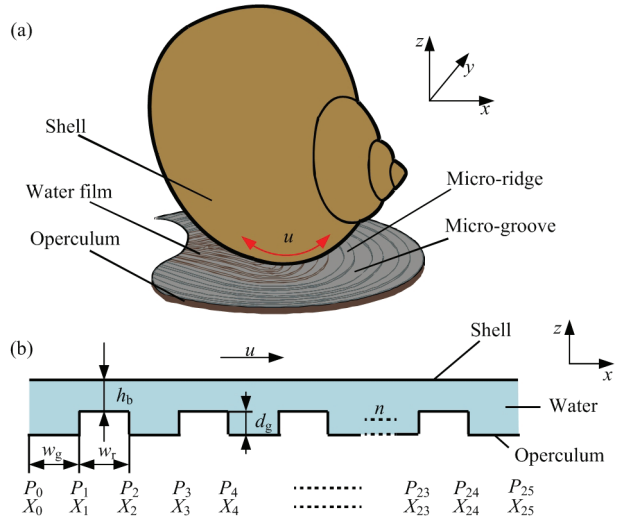

Fig. 5 Hydrodynamic model of friction reduction mechanism of the operculum. (a) A schematic illustration of movement between the shell and operculum; (b) the hydrodynamic model.

u and the number of Rayleigh blocks n = 12 which is selected by length of contact area. The relationship between the line speed u and relative angular velocity ω can be expressed as $u = r\omega$, where r is the curvature radius of shell. Each parameter of the model is given in Table 1.

This model conforms to the Reynolds Equation assumes[26]. Through simplification the general form of Reynolds Equation, we obtain:

$$\frac{\mathrm{d}}{\mathrm{d}x}\left(h_\mathrm{b}^3\frac{\mathrm{d}P}{\mathrm{d}x}\right)=6u\eta\frac{\mathrm{d}h_\mathrm{b}}{\mathrm{d}x}, \tag{3}$$

where P is the fluid pressure[27]. The h_b=Const, so $h_\mathrm{b}^3\frac{\mathrm{d}^2P}{\mathrm{d}x^2}=0$. Then the pressure for one micro-groove is $P=C_1x+C_2$ and for one micro-ridge is $P=C_3x+C_4$. The pressure at points A, B, ⋯, Z are P_0, P_1, ⋯, P_{25}, respectively. Moreover, to preserve the mass conservation in the system, the left and right surfaces are set as the velocity-inlet boundary and velocity-outlet boundary respectively, with the boundary condition P_0=P_{25}=0. In addition, we assume that the micro-grooves are distributed evenly. The speed of vertical direction u_z can be described as:

$$u_z=\frac{1}{2\eta}\frac{\partial P}{\partial x}\left(z^2-zh_\mathrm{b}\right)+\frac{uz}{h_\mathrm{b}}-u. \tag{4}$$

So the unit discharge (the unit volume rate of flow) can be expressed by:

$$q_{xi}=\int_0^{h_{bi}}u_z\mathrm{d}z. \tag{5}$$

Depending on the theory of continuous flow

$$Q_{x(i-1)}=Q_{xi}=Q_{x(i+1)}. \tag{6}$$

We can obtain $q_{x(i-1)}=q_{xi}=q_{x(i+1)}$. By solving the Eqs. (3)–(6), we can obtain the pressure of each point as:

$$\begin{cases}P_{2i+1}-P_{2i}=P_{2i-1}-P_{2i-2}\\ P_{2i}-P_{2i-1}=\dfrac{w_\mathrm{r}}{w_\mathrm{g}}\left(\dfrac{h_\mathrm{b}+d_\mathrm{g}}{h_\mathrm{b}}\right)^3(P_{2i-1}-P_{2i-2})+\dfrac{6u\eta w_\mathrm{r}d_\mathrm{g}}{h_\mathrm{b}^3}.\end{cases} \tag{7}$$

Based on the above equations, we can obtain the pressure P in each micro-groove. The pressure makes the water film have a certain carrying capacity F_N, which can be expressed by:

$$F_N=\sum_{i=1}^{n+1}\left[\frac{1}{2}w_\mathrm{g}(P_{2i-1}+P_{2i-2})\right]+\sum_{i=1}^{n}\left[\frac{1}{2}w_\mathrm{r}(P_{2i}+P_{2i-1})\right]. \tag{8}$$

After calculation, the carrying capacity can support the shell when considering water buoyancy. It indicates the water film between the shell and operculum can generate hydrodynamic lubrication to separate them. Moreover, for better analysis of the lubrication mechanism, we solve theoretical friction coefficient f by:

$$f=F_f/F_N. \tag{9}$$

The F_f is the summation of the friction, which can be calculated by:

Table 1 Parameters of the model

Parameter	Description	Value			Unit
		Pomacea canaliculata	*Pomacea bridgesii*	*Bellamya chinensis*	
η	Viscosity of water at 26 °C		8.737×10^{-4}		Pa·s
ρ	Density of the water		1.0×10^{3}		kg·m^{-3}
u	Relative velocity	3.2×10^{-4}	2.3×10^{-4}	3.8×10^{-5}	m·s^{-1}
w_g	Width of the micro-groove	145 ± 30	82 ± 17	57 ± 18	μm
w_r	Width of the micro-ridge	85 ± 25	55 ± 15	66 ± 20	μm
d_g	Depth of the micro-groove	15 ± 4	11 ± 4	14 ± 4	μm

$$F_f = w_g \sum_{i=1}^{n+1} \tau_A + w_r \sum_{i=1}^{n} \tau_B, \tag{10}$$

in which

$$\begin{cases} \tau_A = \dfrac{u\eta}{h_b + d_g} - \dfrac{h_b + d_g}{2}\left(\dfrac{P_{2i-1} - P_{2i-2}}{w_g}\right), \\ \tau_B = \dfrac{u\eta}{h_b} - \dfrac{h_b}{2}\left(\dfrac{P_{2i} - P_{2i-1}}{w_r}\right) \end{cases} \tag{11}$$

3.5 Friction reduction

The theoretical friction coefficient f is calculated by using Matlab. We define the ratio of the water film's thickness to the micro-groove's depth as V, which can be expressed as $V=h_b/d_g$. The parameter V is nondimensional to describe the relationship between the water film thickness and the depth of micro-grooves. Fig. 6 shows the influence of the ratio V on the theoretical friction coefficient f of *P. canaliculata*. As shown in Fig. 6a, theoretical friction coefficient f as a function of the ratio V is examined at three specified values of w_r and w_g. We find that under different w_r and w_g, theoretical friction coefficient f first decreases remarkably and then increases with the increases of V. Thus, there is an optimal value of V for each given value of w_r, w_g leading to a great decline of the f for a fixed h_b (8 μm). Geometrical parameters of the micro-grooves on operculum have a pronounced influence to the friction coefficient. Fig. 6a shows that the optimal values of ratio V = 0.57 μm, 0.62 μm, 0.66 μm can minimize friction coefficient f into 0.0028, 0.0096, 0.0115, respectively. In addition, the optimal value shifts to a higher V value as the micro-groove's width increases, and the minimum friction coefficient rising gradually with increment of the micro-groove's width. Depicted in Fig. 6a, the dots suggest that our experimental subject namely *P. canaliculata* which have V = 0.72, 0.53 and 0.42, are close to the theoretically-optimal values. Calculation shows that the actual friction coefficient between operculum and shell varies from 0.0056 to 0.0210 (the shading in Fig. 6a) which suggests *P. canaliculata* have the geometric parameters of the operculum's micro-grooves for friction reduction. Additional simulations are performed with w_r=85 μm and w_g=145 μm, namely, the average micro-grooves dimensions of *P. canaliculata*. The results of the theoretical friction coefficient f against V for different values of water film thickness h_b are shown in Fig. 6b. The overall trend of each curve is similar to the ones in Fig. 6a and the ratio V influence on theoretical friction coefficient is similar. This figure clearly shows that when the ratio V is about 0.6, the optimal friction reduction performance can be obtained. *P. canaliculata* have V = 0.53 making the friction coefficient equals 0.011 when the water film thickness is taken as 8 μm. However, a comparison of the theoretical friction coefficient value reveals that a small water film thickness generates a greater carrying capacity to reduce friction coefficient compared with a large water film thickness at the optimum V values.

We extensively compared the friction coefficient among three species of water snails with the ratio V at h_b=8 μm (Fig. 7). Curves of this figure are drawn for snails of *P. canaliculate*, *P. bridgesii* and *B. chinensis*. It can be seen that the highest friction coefficient is in operculum-shell of *B. chinensis* and the lowest value can be found in *P. canaliculata*. For *P. canaliculata* and *P. bridgesii*, the experimental values of V are close to individual theoretically-optimal value (V = 0.62 and 0.72, respectively), which reduce friction coefficient f to 0.012 ± 0.003 and 0.036 ± 0.005. Nevertheless, *B. chinensis* have experimental V = 0.44 – 0.80 which the friction coefficient is 0.16 ± 0.03. It can be found the friction coefficient is more than ten times of that of *P. canaliculata*. This difference might result mainly from behavioral diversity of water snails. The snails, *B. chinensis*, have a thick shell and prefer burying themselves in muddy or silty bottoms[28]. From our observation and calculation, *B. chinensis* are far less active than two other species of water snail, and the average relative angular velocity between the shell and operculum is merely 0.37 °·s^{-1}, therefore the friction coefficient like this is reasonable. Fig. 7 also demonstrates the potential of friction reduction with the textured surface as compared to smooth surface where d_g=0. When h_b is constant, the depth of the micro-groove d_g changes inversely with the ratio V. For *P. canaliculata*, *P. bridgesii* and *B. chinensis*, the reduction of the friction coefficient are 97%, 95% and 77%, respectively, which as the ratio decrease from V = 8 (d_g = 1 μm, close to the smooth surface) to experimental value. It should be noted that

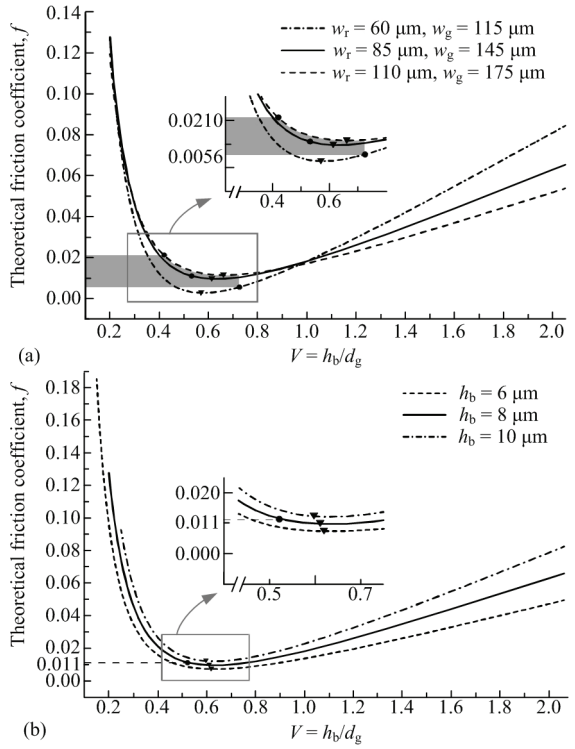

Fig. 6 Mapping of theoretical friction coefficient f against the ratio V (*P. canaliculata*). (a) Under different values of w_r and w_g with h_b = 8 μm; (b) under different values of h_b with w_r = 85 μm, w_g= 145 μm. The black triangle marks the ratio V which friction coefficient f reaches the minimum value. The dots are the experimental results.

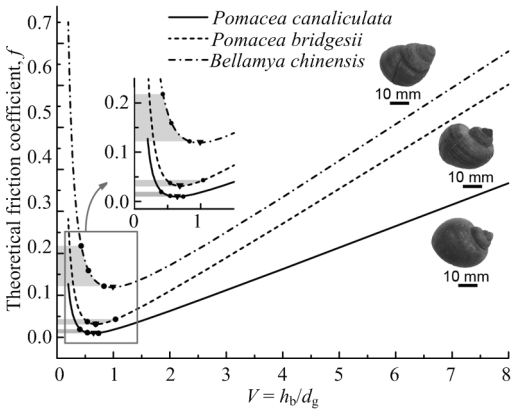

Fig. 7 Mapping of theoretical friction coefficient f against the ratio V for three different species of water snail (*P. canaliculata*, *P. bridgesii* and *B. chinensis*). The black triangle marks the ratio V which friction coefficient f reaches the minimum value. The dots are the experimental results. The shading indicates the error band of the friction coefficient.

this model cannot be used with d_g=0 since no hydrodynamic capacity can be generated in this condition. According to theoretical analysis, the micro-grooves structure of the operculum can generate hydrodynamic pressure, which might be beneficial for friction reduction.

The friction reduction capability of water snails might have intrinsic connections with their physiological behavior and environmental adaptabilities. *P. canaliculata*, an invasive freshwater snail native to South America[29], was first introduced to China during 1990s[30]. Invasive species are characterized by strong propagation, adaptation to environment and competitive competency, which have caused grave effects on ecosystem function and agricultural production[31]. *P. canaliculata* has large food intake as an invasive species, which can ingest 7 – 24 seedlings per day[32]. We observed that, snails of *P. canaliculata* (n = 5 samples) can spend 3.0 h ± 0.5 h in a day to feed, consuming 0.20 g ± 0.06 g vegetables per hour. Comparatively, *P. bridgesii* (n = 5 samples) spend 3.5 h ± 0.5 h per day for feeding, and the food consumption rate is 0.16 $g \cdot h^{-1}$ ± 0.05 $g \cdot h^{-1}$, which similar to that of *P. canaliculata*. *B. chinensis* (n = 5 samples), spend 0.5 h ± 0.2 h per day for feeding, and the food consumption rate is 0.05 $g \cdot h^{-1}$ ± 0.02 $g \cdot h^{-1}$, which is 4 times less than that of *P. canaliculata*. The data were analyzed statistically for differences in crawling time and food consumption rate using one-way ANOVA by SPSS (V22.0, IBM, USA). As shown in Table 2, there are no significant differences in crawling time and food consumption rate among *P. canaliculata* and *P. bridgesii* (p>0.05), whereas highly significant difference in *B. chinensis* among the other two species (p<0.05). Theoretical analysis indicates that, water snails, *P. canaliculata*, perform best in drag reduction, which is beneficial for protecting their functional appendages. From the perspective of foraging duration and food consumption rate, we reveal that, the micro-texture-facilitated drag reduction might enhance the feeding performance, further improve its growth rate and environmental adaptability.

Animals have a variety of strategies to reduce friction in joints and connecting tissues. Some sealed joints, such as articulations of mammals, have mucus secreted by surrounding glands which can help reduce friction[33]. For some opened joints, such as rotary joints in insect appendages, might have micro-patterns on the contact surface to aid in wear reduction[19]. For aquatic animals, dolphins are well streamlined with body dimensions to reduce pressure drag[34]. The surface microstructure of fish scales was revealed responding to skin friction drag

Table 2 Multiple comparisons of three water snail species (n=5, each species)

Species		Crawling time (h)			Food consumption rate ($g \cdot h^{-1}$)		
		M.D.	S.E.	p	M.D.	S.E.	p
P. canaliculata	*P. bridgesii*	−0.426	0.286	0.162	0.040	0.294	0.200
	B. chinensis	2.576*	0.286	0.000	0.142*	0.294	0.000
P. bridgesii	*P. canaliculata*	0.426	0.286	0.162	−0.398	0.294	0.200
	B. chinensis	3.002*	0.286	0.000	0.102*	0.294	0.005
B. chinensis	*P. canaliculata*	−2.576*	0.286	0.000	−0.142*	0.294	0.000
	P. bridgesii	−3.002*	0.286	0.000	−0.102*	0.294	0.005

Note. M.D.: Mean Difference; S.E.: Std. Error; *p<0.05.

reduction[35]. The mucus of many fishes assist in locomotion by reducing the drag which water offers to their bodies[36]. The micro-riblets on the surface of shark skin can prevent the formation of vortices, which possess the drag reduction performance[37]. For water snails, the habitat provides a good chance for the animals to use both water and micro-grooves to form an effective hydrodynamic lubrication.

4 Conclusion

In this combined theoretical and experimental investigation, we discovered the micro-grooves are concentrically distributed on the outer surface of the operculum and measured three species water snail's dimensions of the micro-grooves. Furthermore, the simulation results of dry friction illustrate that the shell rotation on the operculum without water can cause wear compared with natural physiological conditions. Inspired by this, a hydrodynamic lubrication model was established to analyze the effect of friction reduction caused by the micro-grooves of the operculum. We found that *P. canaliculata* and *P. bridgesii* have greater reduction in the friction coefficient compared to *B. chinensis*, which probably relates to their different life history traits. The results of theoretical friction coefficient validate that the water snails have an optimal value of the depth of the micro-grooves which administer to friction reduction. The specific microstructure of the operculum provides new insights, which might facilitate the design and fabricate micro-anti-wear structure used in water and other liquid media.

Acknowledgment

We thank the Centre of Biomedical Analysis of Tsinghua University. This study was funded by the National Natural Science Founding of China (Grant no. 51475258) and the Research Project of the State Key Laboratory of Tribology under Contract SKLT2014B06.

* All supplementary materials are available at http://www.springer.com/journal/42235.

References

[1] Carlsson N O L, Bronmark C. Size-dependent effects of an invasive herbivorous snail (*Pomacea canaliculata*) on macrophyte and periphyton in Asian wetlands. *Freshwater Biology*, 2006, **51**, 695–704.

[2] Seuffert M E, Burela S, Martin P R. Influence of water temperature on the activity of the freshwater snail *Pomacea canaliculata* (Caenogastropoda: Ampullariidae) at its southernmost limit (Southern Pampas, Argentina). *Journal of Thermal Biology*, 2010, **35**, 77–84.

[3] Harrision F W, Kohn A J. *Microscopic Anatomy of Invertebrates*, *Volume* 5, *Mollusca I*, Wiley-Liss, New York, USA, 1994.

[4] Páll-Gergely B, Naggs F, Asami T. Novel shell device for gas exchange in an operculate land snail. *Biology Letters*, 2016, **12**, 20160151.

[5] Poznańska M, Kakareko T, Gulanicz T, Jermacz Ł, Kobak J. Life on the edge: Survival and behavioural responses of freshwater gill-breathing snails to declining water level and substratum drying. *Freshwater Biology*, 2015, **60**, 2379–2391.

[6] Chen Y, Wang X, Ren H, Yin H, Jia S. Hierarchical dragonfly wing: Microstructure-biomechanical behavior relations. *Journal of Bionic Engineering*, 2012, **9**, 185–191.

[7] Rajabi H, Shafiei A, Darvizeh A, Dirks J, Appel E, Gorb S N. Effect of microstructure on the mechanical and damping behaviour of dragonfly wing veins. *Royal Society of Open Science*, 2016, **3**, 160006.

[8] Liang Y, Zhao J, Yan S. Honeybees have hydrophobic wings that enable them to fly through fog and dew. *Journal of Bionic Engineering*, 2017, **14**, 549–556.

[9] Yang Y, Wu J, Zhu R, Li C, Yan S. The honeybee's protru-

sible glossa is a compliant mechanism. *Journal of Bionic Engineering*, 2017, **14**, 607–615.

[10] Bhushan B. Biomimetics: Lessons from nature—an overview. *Philosophical Transactions*, 2009, **367**, 1445–1486.

[11] Li C, Wu J, Yang Y, Zhu R, Yan S. Drag reduction in the mouthpart of a honeybee facilitated by galea ridges for nectar-dipping strategy. *Journal of Bionic Engineering*, 2015, **12**, 70–78.

[12] Wu J, Yang H, Yan S. Energy saving strategies of honeybees in dipping nectar. *Scientific Reports*, 2015, **5**, 15002.

[13] Wu J, Zhu R, Yan S, Yang Y. Erection pattern and section-wise wettability of honeybee glossal hairs in nectar feeding. *Journal of Experimental Biology*, 2015, **218**, 664–667.

[14] Gu Y Q, Fan T X, Mou J G, Jiang L F, Wu D H, Zheng S H. A review of bionic technology for drag reduction based on analysis of abilities the earthworm. *International Journal of Engineering Research in Africa*, 2015, **19**, 103–111.

[15] Wainwright S A, Vosburgh F, Hebrank J H. Shark skin: Function in locomotion. *Science*, 1978, **202**, 747–749.

[16] Tian L, Jin E, Mei H, Ke Q, Li Z, Kui H. Bio-inspired graphene-enhanced thermally conductive elastic silicone rubber as drag reduction material. *Journal of Bionic Engineering*, 2017, **14**, 130–140.

[17] Oeffner J, Lauder G V. The hydrodynamic function of shark skin and two biomimetic applications. *Journal of Experimental Biology*, 2012, **215**, 785–795.

[18] Jung Y C, Bhushan B. Biomimetic structures for fluid drag reduction in laminar and turbulent flows. *Journal of Physics Condensed Matter An Institute of Physics Journal*, 2010, **22**, 035104.

[19] Han Z, Zhu B, Yang M, Niu S, Song H, Zhang J. The effect of the micro-structures on the scorpion surface for improving the anti-erosion performance. *Surface & Coatings Technology*, 2017, **313**, 143–150.

[20] Shi G, Wu J, Yan S. Drag reduction in a natural high-frequency swinging micro-articulation: Mouthparts of the honey bee. *Journal of Insect Science*, 2017, **17**, 1–7.

[21] Eleutheriadis N, Lazaridoudimitriadou M. The life cycle, population dynamics, growth and secondary production of Bithynia graeca (Westerlund, 1879) (Gastropoda) in Lake Kerkini, Northern Greece. *Journal Molluscan Studies*, 2001, **67**, 319–328.

[22] Chandrasekaran T, Kishore. On the roughness dependence of wear of steels: A new approach. *Journal of Materials Science Letters*, 1993, **12**, 952–954.

[23] Duvvuru R S, Jackson R L, Hong J W. Self-adapting microscale surface grooves for hydrodynamic lubrication. *Tribology Transactions*, 2008, **52**, 1–11.

[24] Li C C, Wu J N, Yang Y Q, Zhu R G, Yan S Z. Drag reduction effects facilitated by microridges inside the mouthparts of honeybee workers and drones. *Journal of Theoretical Biology*, 2016, **389**, 1–10.

[25] Ikeuchi K, Mori H, Nishida T. A face seal with circumferential pumping grooves and rayleigh-steps. *Transactions of the Japan Society of Mechanical Engineers C*, 1988, **110**, 313–319.

[26] Reynolds O. On the theory of lubrication and its application to Mr. Beauchamp tower's experiments, including an experimental determination of the viscosity of olive oil. *Proceedings of the Royal Society of London*, 1886, **40**, 191–203.

[27] Siripuram R B, Stephens L S. Effect of deterministic asperity geometry on hydrodynamic lubrication. *Journal of Tribology*, 2004, **126**, 527–534.

[28] Jokinen E H. *Cipangopaludina chinensis* (Gastropoda: Viviparidge) in North America, review and update. *Nautilus*, 1982, **96**, 89–95.

[29] Lopes H S. Sôbre *Pomacea canaliculata* (Lamarck, 1822) (Mesogastropoda, Architaenioglossa, Mollusca). *Revista Brasileira de Biologia*, 1956, **16**, 535–542. (in Portuguese)

[30] Carlsson N O L, Brönmark C, Hansson L A. Invading herbivory: The golden apple snail alters ecosystem functioning in Asian wetlands. *Ecology*, 2004, **85**, 1575–1580.

[31] Kolar C S, Lodge D M. Progress in invasion biology: Predicting invaders. *Trends in Ecology & Evolution*, 2001, **16**, 199–204.

[32] Oya S, Hirai Y, Miyahara Y. Injuring habits of the apple snail, *Ampullarius insularus* D'Orbigny, to the young rice seedlings. *Kyushu Plant Protection Research*, 1986, **32**, 92–95.

[33] Linn F C. Lubrication of animal joints. I. The arthrotripsometer. *Journal of Bone & Joint Surgery-American Volume*, 1967, **49**, 1079–1098.

[34] Fish F E. Imaginative solutions by marine organisms for drag reduction. *Proceedings of the International Symposium on Seawater Drag Reduction*, 1998, 443–450.

[35] Dou Z, Wang J, Chen D. Bionic research on fish scales for drag reduction. *Journal of Bionic Engineering*, 2012, **9**, 457–464.

[36] Rosen M W, Cornford N E. Fluid friction of fish slimes. *Nature*, 1971, **234**, 49–51.

[37] Zhao D, Tian Q, Wang M, Jin Y. Study on the hydrophobic property of shark-skin-inspired micro-riblets. *Journal of Bionic Engineering*, 2014, **11**, 296–302.